Bioinspired Graphene Nanopores with Voltage-Tunable Ion Selectivity for Na^+ and K^+

Zhongjin He,[†,§] Jian Zhou,[†,*] Xiaohua Lu,[‡] and Ben Corry[§,*]

[†]School of Chemistry and Chemical Engineering, South China University of Technology, Guangzhou, Guangdong 510640, China, [‡]State Key Laboratory of Materials-Oriented Chemical Engineering, Nanjing University of Technology, Nanjing 210009, China, and [§]Research School of Biology, The Australian National University, Canberra ACT 0200, Australia

ABSTRACT Biological protein channels have many remarkable properties such as gating, high permeability, and selectivity, which have motivated researchers to mimic their functions for practical applications. Herein, using molecular dynamics simulations, we design bioinspired nanopores in graphene sheets that can discriminate between Na^+ and K^+, two ions with very similar properties. The simulation results show that, under transmembrane voltage bias, a nanopore containing four carbonyl groups to mimic the selectivity filter of the KcsA K^+ channel preferentially conducts K^+ over Na^+. A nanopore functionalized by four negatively charged carboxylate groups to mimic the selectivity filter of the NavAb Na^+ channel selectively binds Na^+ but transports K^+ over Na^+. Surprisingly, the ion selectivity of the smaller diameter pore containing three carboxylate groups can be tuned by changing the magnitude of the applied voltage bias. Under lower voltage bias, it transports ions in a single-file manner and exhibits Na^+ selectivity, dictated by the knock-on ion conduction and selective blockage by Na^+. Under higher voltage bias, the nanopore is K^+-selective, as the blockage by Na^+ is destabilized and the stronger affinity for carboxylate groups slows the passage of Na^+ compared with K^+. The computational design of biomimetic ion-selective nanopores helps to understand the mechanisms of selectivity in biological ion channels and may also lead to a wide range of potential applications such as sensitive ion sensors, nanofiltration membranes for Na^+/K^+ separation, and voltage-tunable nanofluidic devices.

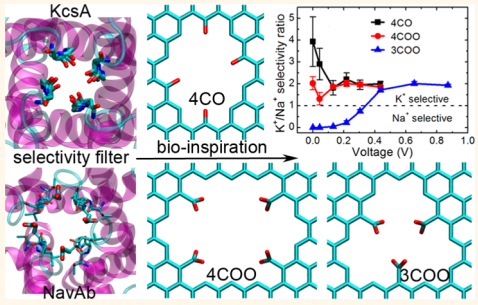

KEYWORDS: graphene · nanopores · ion channel · molecular dynamics · ion selectivity · nanofluidics

Through millions of years of evolution, biological protein channels have developed many remarkable properties and can provide a great source of inspiration for the development of biomimetic nanopores. These channel proteins transport substances across membranes in cells and are able to achieve extremely high permeability simultaneously with exquisite selectivity in order to realize a variety of functions essential to life.[1] For example, protein water channels are able to achieve rapid water fluxes while rejecting ions,[2] and some ion channel proteins are able to discriminate between very similar ion types by a factor of over 1000 and can display current rectification.[3] Moreover, these channels are able to open and close their ion conduction pathways in response to external stimulation and so can respond to their environment.[1] The remarkable features of biological channel proteins have sparked tremendous experimental and theoretical efforts to utilize these properties in technological applications.[4−13] However, the mechanical properties of these proteins are quite poor, and they often lose bioactivity when leaving the biological setting, which has limited their use in technological applications. Therefore, it is very interesting to explore whether the key structures and mechanisms of biological channel proteins could be mimicked by synthetic nanopores, which have much simpler structures and stronger mechanical properties, to transplant their functions to practical applications. Biomimetic nanopores displaying rapid transport and/or selectivity properties have a wide range of potential applications, such as in the desalination of seawater, in nanofluidic devices, in ultrasensitive biosensors, and in biomedical diagnostics.

Graphene is a two-dimensional sheet of sp^2-bonded carbon atoms in a hexagonal

* Address correspondence to jianzhou@scut.edu.cn, ben.corry@anu.edu.au.

Received for review August 20, 2013 and accepted October 23, 2013.

Published online October 23, 2013
10.1021/nn4043628

honeycomb lattice with atomic thickness and high mechanical strength.[14] Holes or defects in graphene as small as 0.3 nm in radius, known as graphene nanopores, can appear naturally during synthesis[15] or can be produced by means of etching, ion, or electron bombardment[16,17] and have a variety of potential applications. First principle calculations[18,19] and experimental work[20] demonstrated that angstrom-sized pores in graphene are capable of selective molecular sieving for gas separation. Molecular dynamics (MD) simulation results of Cohen-Tanugi *et al.*[21] indicated that functionalized nanopores with proper diameters could separate NaCl salt from water, which may be an effective means of water desalination. Wastewater purification may be achieved by graphene oxide membranes, which are able to remove heavy-metal salts and organic contaminants from water.[22] The theoretical work of Sint *et al.*[23] suggested that the graphene nanopores could be tuned to selectively transport cations or anions by chemical modification. In addition, graphene nanopores have been investigated as a novel approach to DNA sequencing.[24−28] Therefore, graphene is an attractive material for the biomimetic design of nanopores.

Having an understanding of the structures and mechanisms of biological channel proteins is essential if we are to transplant their properties to nanopores. In this work, we focus on the selective passage of either Na^+ or K^+, which underlies electrical signaling in the nervous system.[1] It is generally considered quite difficult to distinguish between Na^+ and K^+ ions, as they are both alkali cations with the same charge, similar hydration properties, and ionic radii. However, biological K^+ channels have the ability to discriminate K^+ from Na^+ by up to 1000-fold,[1,29] whereas the Na^+ channels can select Na^+ over K^+ with an efficiency of up to 100:1.[30,31] The recently determined crystal structures of a voltage-gated prokaryotic sodium channel from *Arcobacter butzleri*[31] (NavAb) and a potassium channel from *Streptomyces lividans*[32] (KcsA) along with a number of additional structures[33−36] provide a basis for rationalizing the physical foundation of ion selectivity. Both are formed from a tetrameric arrangement of protein chains and include a narrow pore region (selectivity filter) known to dictate ion selectivity. The selectivity filter of the KcsA K^+ channel is lined by four rings of backbone carbonyl groups (Figure S1 in the Supporting Information). When K^+ and Na^+ enter into the narrow filter, they are almost completely dehydrated and the carbonyl groups partially compensate for this effect, albeit to a greater extent for K^+ than Na^+.[3] The exact reason why this compensation is better for K^+ than Na^+ is still a hot topic of research. It may include "topological" factors, such as the size and flexibility of the pore, the chemical nature of the pore lining, the coordination numbers accessible to ions in the pore, as well as the kinetic consequences of multi-ion conduction.[37−44] The selectivity filter of the NavAb Na^+ channel is shorter and wider than that of KcsA and is composed of a ring of four negatively charged carboxylate groups from the Glu177 side chains and two rings of backbone carbonyl groups from Thr175 and Leu176.[31] The four carboxylate groups of the Glu177 side chains form a relatively rigid square-like structure stabilized by hydrogen bonds with other residues (Figure S1 in the Supporting Information). In the plane of four carboxylate groups, Na^+ binds to one carboxylate, and two water molecules form water bridges between Na^+ and two neighboring carboxylates; K^+ and Ca^{2+} cannot form such favorable coordination structures and are disfavored in the pore.[31,45−47] In addition, the determinants governing Na^+ or K^+ selectivity have been systematically explored in simplified model systems.[37,39,40,48−54]

Inspired by the selectivity filters of NavAb Na^+ channel and KcsA K^+ channel, in this work, we design biomimetic Na^+- or K^+-selective graphene nanopores using MD simulations by altering the pore size and the chemical nature of the pore rim. The unambiguous goal is to achieve larger flow of the selected ion (selective conduction) through the nanopores as is required for practical applications, not just to show differences in the free energy landscape of the ions[9] or differences in ion−nanopore interactions (selective binding).[10] The successful design of biomimetic Na^+- or K^+-selective graphene nanopores here may help elucidate the essential ingredients required to generate selectivity for each ion type and provide the basis for fabricating materials for potential applications.

RESULTS AND DISCUSSION

Bioinspired Graphene Nanopores. A certain number of carbon atoms in the center of a 3.20 × 3.27 nm^2 graphene sheet were removed to form biomimetic nanopores. Three nanopores were designed, as shown in Figure 1A. Four carbonyl groups were attached to the 4CO nanopore, ~0.65 nm in diameter, to mimic one out of the four layers of carbonyl groups in the KcsA selectivity filter (Figure 1B). The 4COO nanopore was functionalized with four negatively charged carboxylate groups with a diameter of ~0.79 nm, inspired by side chains of the four glutamate residues in the NavAb selectivity filter (Figure 1B). Three carboxylate groups were attached to the 3COO nanopore, and its diameter was 0.43 nm. To make the 4CO, 4COO, and 3COO nanopores, 16, 32, and 22 carbon atoms were removed from the graphene sheet, respectively. Nanopores in graphene sheets can be punched by electron beam[16] or ion etching,[17] and local oxidation could be used to functionalize the pore rims.[55] While these methods can typically only produce pores of diameter greater than 2−5 nm, here we show that a smaller pore size is critical to generating ion selectivity. However, a recent report suggests that the size of the graphene

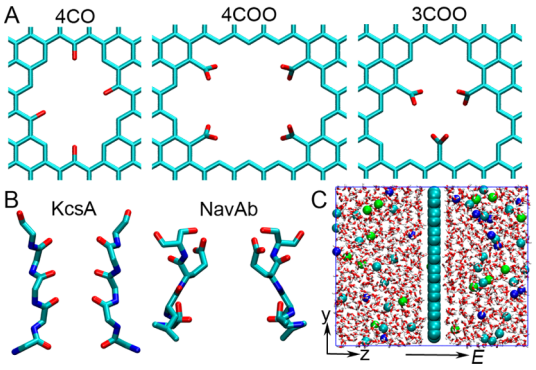

Figure 1. Graphene nanopores, biological inspiration, and simulation system. (A) The 4CO, 4COO, and 3COO nanopores are modified with four carbonyl, four carboxylate, and three carboxylate groups, respectively. Each carboxylate group carries a net charge of −1 *e*. (B) Selectivity filter of the KcsA K^+ channel consists of 16 backbone carbonyl groups. The selectivity filter of the NavAb Na^+ channel contains four carboxylate groups from glutamate residues side chains. For clarity, only two out of four subunits are depicted for each. (C) Simulation system. The graphene sheet is in cyan. Water molecules are depicted as red and white rods. The blue, green, and cyan balls represent Na^+, K^+, and Cl^-, respectively. For some simulations, a transmembrane voltage bias *V* is applied to generate a uniform electric field *E* along the positive direction of the *z*-axis.

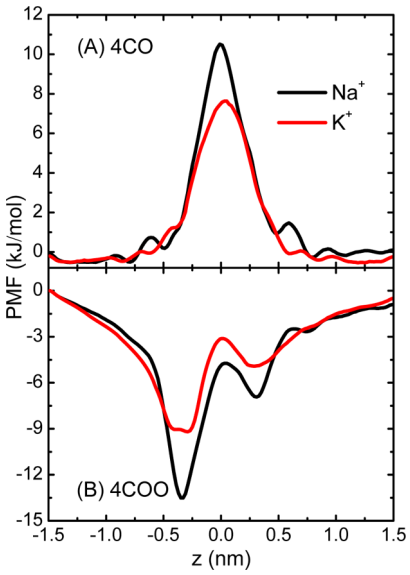

Figure 2. One-dimensional PMF for Na^+ and K^+ traversing through (A) 4CO and (B) 4COO nanopores. The graphene sheet is at *z* = 0.

nanopore can be tailored through a combination of electron beam irradiation and controlled heat.[56] Therefore, there is hope that very small pores such as those described in this work will be fabricated in the near future.

Energetics of Na^+ and K^+ Permeation through the Nanopores. The ion selectivity of the nanopores was first explored by calculation of potential of mean force (PMF), that is, the free energy profiles of an ion passing through the nanopores. The two-dimensional and one-dimensional PMF profiles for Na^+ and K^+ passing through the 4CO and 4COO nanopores are shown in Figure S2 in the Supporting Information and Figure 2, respectively. All the PMF profiles should be considered as single-ion PMFs as other ions were not present in the nanopore during the umbrella sampling simulations. The 4CO nanopore provides a larger and lower free energy region for K^+ than Na^+ (Figure S2A,B in the Supporting Information). The energy barrier of Na^+ transiting through the 4CO graphene nanopore is 2.9 kJ/mol higher than that of K^+ (Figure 2A). Therefore, we expect it to be easier for K^+ to pass through the nanopore than Na^+. Recent studies[7,57−63] showed that the hydration state of ions under nanoscale confinement is quite different from that in the bulk.[64] Ion coordination numbers and the type of ligands can have a large influence on ion selectivity.[37−41,50,53,54] Thus, the hydration states of the ions were analyzed to assess the origin of the small energy differences for K^+ and Na^+. During permeation through the 4CO nanopore, some water molecules in the first hydration shells of Na^+ and K^+ are gradually stripped away and replaced by carbonyl groups from the nanopore (Figure S3A,CC in the Supporting Information). In the nanopore, Na^+ is coordinated by about 4.5 water molecules and 1 carbonyl group and K^+ by 4.5 water molecules and 2 carbonyl groups, with 2 or 3 water molecules surrounding them on each side of the graphene sheet (the inset of Figure S3A in the Supporting Information). Compared with that in bulk, Na^+ and K^+ are slightly dehydrated; however, K^+ is coordinated by one more carbonyl oxygen than Na^+, resulting in the K^+ selectivity of the nanopore, which is in line with the prediction of Thomas *et al.* made in model systems.[50] A similar situation is found in the selectivity filter of KcsA, where K^+ is hydrated by two more carbonyl groups than Na^+, though their total coordination numbers are both bulk-like.[65]

Asymmetric energy wells are presented on each side of the 4COO nanopore for both Na^+ and K^+, and the energy wells of Na^+ are deeper than those of K^+ (Figure S2C,D in the Supporting Information). The energy wells on the left are 6.6 kJ/mol (for Na^+) and 4.3 kJ/mol (for K^+) deeper than those on the right, as shown in Figure 2B. The asymmetry originates from the orientations of four carboxylates. The strong repulsive interactions among them make them splay away from the graphene plane, with more carboxylate groups pointing to the left than to the right (the inset of Figure S3B and Figure S4A in the Supporting Information), which creates a more favorable electrostatic environment for cations at the left side of the graphene sheet. Although the carboxylates sample both sides of the graphene sheet in much longer simulations, and much longer simulations would average over all slowly varying carboxylate orientations (Figure S4B in the Supporting Information) and create a symmetrical PMF,

the asymmetric profiles seen here represent the most likely situation found with an electric field as described in the simulations below. The energy wells of Na^+ passing through the 4COO nanopore are −13.5 (left) and −9.2 (right) kJ/mol, about 4.3 and 2.0 kJ/mol deeper than those of K^+. Therefore, Na^+ is expected to bind to the 4COO nanopore more strongly than K^+. This observation agrees well with the classical field strength theory;[66] for example, low-field ligands tend to favor larger cations, whereas high-field ligands tend to favor small ones. In addition, several studies[49,50,53,67−69] also found the preferential binding of Na^+ over K^+ to carboxylate groups. When Na^+ approaches the carboxylate groups, about two water molecules are abruptly removed from the first shell and substituted by two carboxylate oxygen atoms (Figure S3B in the Supporting Information). However, this process occurs more gradually for K^+, and only when K^+ is in line with the carboxylate groups on either side of the graphene is it coordinated by two carboxylate oxygen atoms (Figure S3D in the Supporting Information). Although the dimensions of this channel were designed to match that of the NavAb selectivity filter, the water bridges suggested to be important for creating selectivity in the biological counterpart[46,47] are not seen here. This is largely due to the fact that the carboxylate groups move more freely as no hydrogen bonds are formed to restrain them in one plane. Given the strong interactions between both cations and the carboxylate groups, the 4COO nanopore is anticipated to attract multiple cations during ion conduction.

Ion Conduction through the Nanopores under Different Transmembrane Voltage. Calculations of PMFs and relative binding free energy of ions are extensively used to study the ion selectivity of biological channels, but few MD simulation studies[44,70,71] have directly observed ion conduction due to the extremely high demands for computational resources even though this is the closest way to compare the results with experiment. To directly determine whether the nanopores can selectively conduct Na^+ or K^+, MD simulations of mixed NaCl and KCl solution under different transmembrane voltages (V) were performed. The ionic currents of Na^+ and K^+ flowing through these nanopores are calculated[72,73] and shown in Figure 3, while Figure 4 schematically illustrates the mechanism of ion selectivity in each case. The K^+/Na^+ selectivity ratio was defined as the ratio of the bidirectional flows (sum of the number of ions moving in each direction) of K^+ and Na^+, as it can better describe the selectivity of the nanopores under equilibrium condition and low voltages than the ratio of ionic currents.

Under equilibrium conditions ($V = 0$), the number of spontaneous permeations of K^+ (55) through the 4CO pore is about 4 times of that of Na^+ (14). The ionic currents of Na^+ and K^+ increase with V, while the K^+/Na^+ selectivity ratio is maintained to about 2−3, as shown in Figure 3A,F. Therefore, the 4CO nanopore can selectively transport K^+ over Na^+. The conduction of Na^+ and K^+ through this nanopore is in single-ion form (movie S1 in the Supporting Information). During permeation, Na^+ and K^+ usually interact with one and two carbonyl groups in the nanopore (Figure 4A), respectively, consistent with the observation in umbrella sampling.

Despite being designed to mimic the selectivity filter of NavAb and displaying a greater binding affinity for Na^+ than K^+, the 4COO nanopore does not selectively transport Na^+. As shown in Figure 3B,F, this pore selectively conducts K^+ over Na^+ at a ratio of about 2:1, a little lower than that of the 4CO nanopore. However, the mechanism of K^+ selectivity of the 4COO nanopore is quite different. The size of the 4COO nanopore is large enough that it cannot be blocked by any cation, and multiple cations bind to the nanopore simultaneously. Therefore, cations can pass each other in the nanopore, and their passages do not take place *via* a knock-on mechanism. The stronger binding of Na^+ to the carboxylate groups of the 4COO nanopore, evidenced by a peak in Na^+ number density at these positions (Figure S5 in the Supporting Information) and the reorientation of the carboxylates around Na^+ (Figure 4B and movie S2 in the Supporting Information), slows down the passage of Na^+ compared with that of K^+. Even though Na^+ binds more strongly than K^+ in this pore, it does not achieve Na^+ selectivity as K^+ can bypass bound Na^+ ions. Can we create a Na^+-selective pore by utilizing the preferential binding on Na^+ but preventing ions from passing each other? We designed the 3COO nanopore with smaller diameter to address this question.

As shown in Figure 3C−F, the 3COO nanopore exhibits different ion selectivity under low voltages and high voltages. Under low V, Na^+ is selectively conducted by this nanopore (Figure 3C and Figure S6A in the Supporting Information for V = 0.3052 V (E = 0.07 V/nm)). For V = 0, 0.0436, 0.1308, and 0.218 V (E = 0, 0.01, 0.03, and 0.05 V/nm), a longer simulation (1000 ns) was performed to ensure enough sampling of ion passage events through the 3COO nanopore. The passage rate of Na^+ to K^+ is 4.55:1 for $V = 0.218$ V ($E = 0.05$ V/nm). For $V = 0.1308$, 0.0436, and 0 V ($E = 0.03$, 0.01, and 0 V/nm), the number of passage events for Na^+ and K^+ are 48, 13, 8 and 2, 0, 0, respectively, indicating that the Na^+/K^+ selectivity of this nanopore increases with the decreasing V.

Ion conduction through the 3COO nanopore under low V shows unusual features. Conduction takes place *via* a knock-on mechanism (movie S3 in the Supporting Information), as occurs in a number of biological ion channels. Unlike in NavAb, the 3COO nanopore is blocked by the cation in its center and ions cannot pass each other, as the strong attraction from the cation in the nanopore makes the three carboxylate

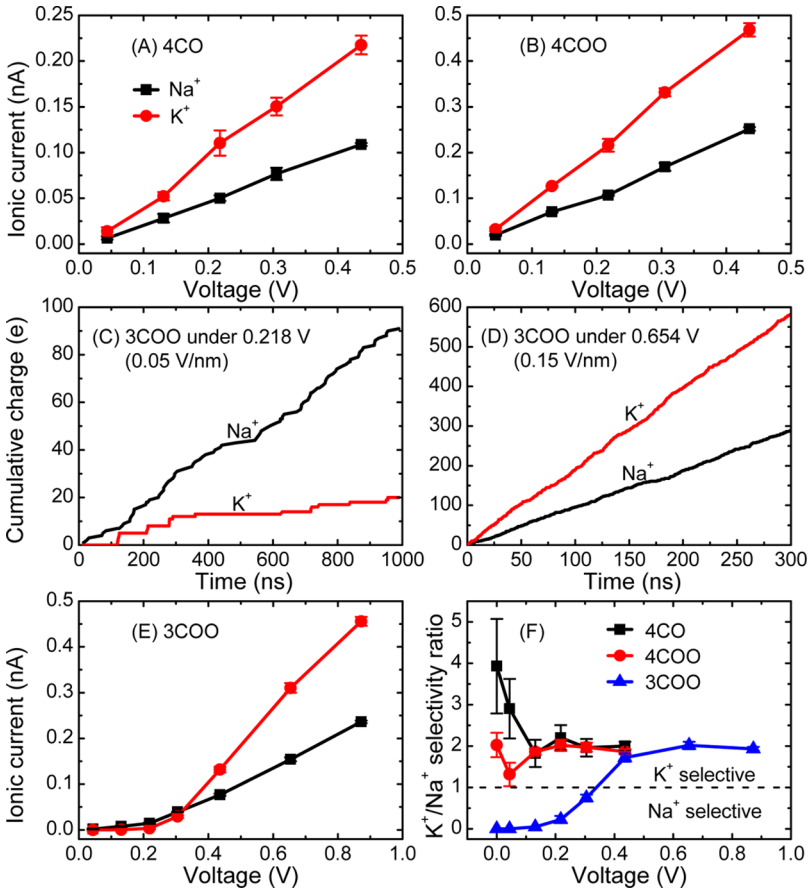

Figure 3. Ionic currents of Na^+ and K^+ through (A) 4CO, (B) 4COO, and (E) 3COO nanopores, the cumulative charge of Na^+ and K^+ through the 3COO nanopore under (C) V = 0.218 V and (D) V = 0.654 V and (F) K^+/Na^+ selectivity ratio of each nanopore under different transmembrane voltages. The currents of Cl^- were always zero for these nanopores.

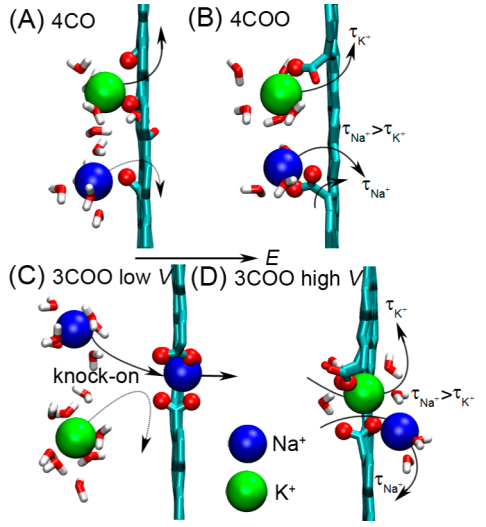

Figure 4. Schematic illustration of the mechanisms of ion selectivity of (A) 4CO, (B) 4COO, and (C,D) 3COO nanopores under low and high transmembrane voltages. The time needed for a Na^+ and a K^+ to pass through the nanopores is τ_{Na^+} and τ_{K^+}, respectively. The blue and green balls represent Na^+ and K^+, respectively.

groups stay in the plane of the graphene sheet (Figure 4C). As a result, cations conduct in a single-file manner. The strong binding of Na^+ to the carboxylate groups and the smaller size of Na^+ which just fits in the plane of nanopore create a more stable ion−nanopore complex than with K^+. As a consequence, the pore is preferentially blocked by Na^+, and it is much easier for the resident ion to be displaced by another Na^+ than by K^+, as shown schematically in Figure 4C, which ultimately yields the observed ion selectivity. Nevertheless, the stronger binding of Na^+ means that the time taken for a single conduction event is longer for Na^+ than for K^+. The effect of ion concentration on ion conduction through the 3COO nanopore under low V should be noted. When the ion concentration is very low, the ion conduction event will not take place, as the repulsion force of another cation during the knocking-on process is required to overcome the strong affinity force of carboxylate groups on the cation to achieve the ion conduction.

Remarkably, under high V (0.436, 0.654, and 0.872 V) (E = 0.1, 0.15, and 0.2 V/nm), the 3COO nanopore is switched to selectively conduct K^+ over Na^+ (with a selectivity ratio of about 2:1), as shown in Figure 3D−F and Figure S6B,C in the Supporting Information. The reason for this change in selectivity is that both the position of the carboxylate groups and the most

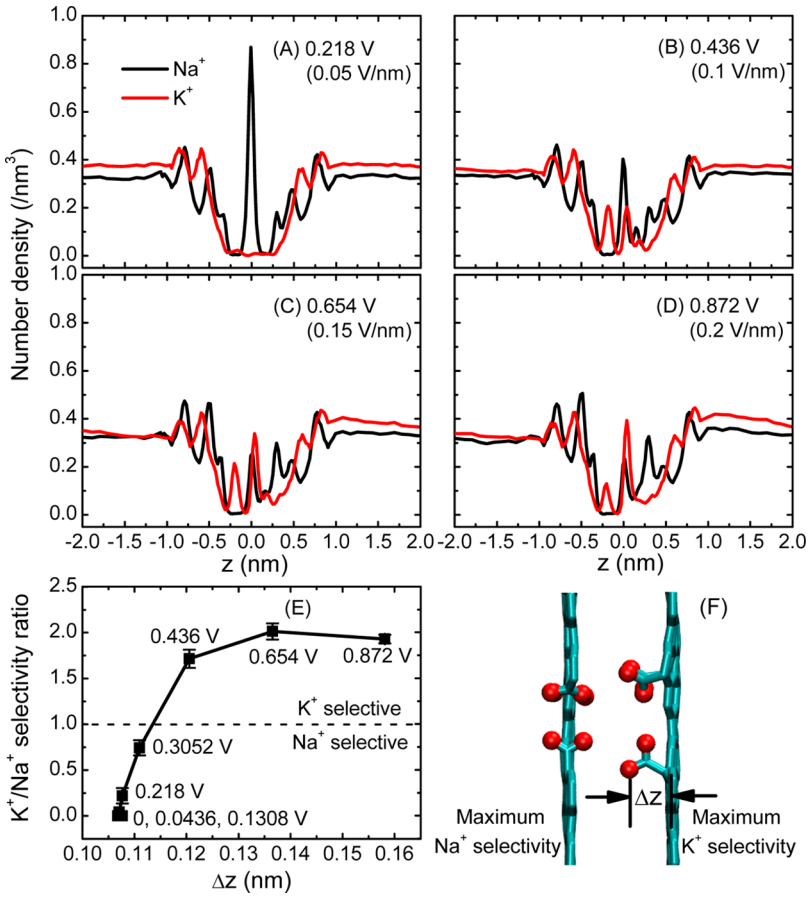

Figure 5. Number density of Na^+ and K^+ along the 3COO nanopore axis (z) under an applied transmembrane voltage V of (A) 0.218, (B) 0.436, (C) 0.654, and (D) 0.872 V. The graphene sheet is at $z = 0$. The dependence of the K^+/Na^+ selectivity ratio on the relative position of carboxylate groups to the graphene sheet (E) and the conformations with the maximum Na^+ and K^+ selectivity (F).

favored binding positions of the ions change in response to the electric field. The carboxylate groups tend to swing out of the graphene plane (Figure 4D and Figure S7C in the Supporting Information), which destabilizes the binding of Na^+. In this situation, Na^+ cannot block the pore as tightly as under low V. As a consequence, K^+ can displace a resident Na^+ ion and pass across the nanopore easily, while Na^+ sticks to the carboxylate group on the right side of the graphene and takes much longer to leave, as shown in Figure 4D and movie S4 in the Supporting Information. The stronger binding of Na^+ to carboxylate groups slows down its passage, similar to the situation in the 4COO nanopore. A change in selectivity ratio has been seen in simulations of the biological channel NavMs which showed approximately a 15-fold preference for Na^+ over K^+ under low voltages but only a 2.5-fold preference under high voltages.[71]

Another way to explore the selectivity change of the 3COO pore with voltages is to calculate the number density of Na^+ and K^+ along the nanopore axis (z), shown in Figure 5. The passage of ions through the graphene nanopores includes two processes: entry into the nanopore from the left side of graphene and exit from the nanopore from the right side of graphene. Increasing V makes it easier for K^+ to enter into the nanopore (evidenced by the increase of the K^+ peak height at $z = 0$). It becomes more difficult for Na^+ to get into and block the nanopore (evidenced by the decrease of the Na^+ peak height at $z = 0$) and more difficult to leave the nanopore (evidenced by the increase of the Na^+ peak height at $z = 0.3$) when increasing the voltage. As a consequence, the selectivity of the nanopore is gradually switched from favoring Na^+ to preferring K^+. In addition, the selectivity change of the 3COO nanopore is closely correlated to the deformation of the carboxylate groups at the pore rim induced by the high voltages, as shown in Figure 5E,F. Under low voltages (0, 0.0436, 0.1308 V), the carboxylate groups stay in the plane of the graphene sheet and show the largest Na^+ selectivity. Under high voltages (0.654 and 0.872 V), the strong driving force of the electric fields makes the carboxylate groups swing out of the graphene plane, and the maximum K^+ selectivity is obtained when this deformation is greatest.

Comparing the results in the three nanopores allows us to identify some of the critical factors for

creating ion selectivity. In general, it appears easier to make the graphene nanopores selective for K^+ than Na^+, which is probably due to K^+ leaving bulk water more easily due to its lower hydration energy[58,61,64] and Na^+ tending to be slowed by stronger interactions to charged or polar groups in the pore. To make a Na^+-selective pore, we found it essential that (i) the pore is small enough that ions cannot pass each other, (ii) Na^+ binds more strongly than K^+ in the pore, and (iii) conduction takes place in a knock-on rather than single-ion fashion. Surprisingly, the filter of NavAb does not meet all these criteria as ions are able to pass each other,[46,71,74−76] but there are also a number of other factors at play in this pore such as structural constraints on key chemical groups and the longer length and more complex environment of the filter.

CONCLUSIONS

We have designed three biomimetic Na^+- or K^+-selective graphene nanopores based on MD simulations. Under a transmembrane voltage bias, the 4CO nanopore, which mimics the KcsA selectivity filter, selectively conducts K^+ over Na^+, as Na^+ encounters an ≈2.9 kJ/mol higher energy barrier than K^+, while the 4COO nanopore, mimicking the NavAb selectivity filter, selectively binds Na^+ but selectively transports K^+ over Na^+, due to its stronger affinity (by 4.3 kJ/mol) for Na^+. The 3COO nanopore shows a voltage-dependent selectivity: the passage of Na^+ is favored with a low voltage as a consequence of the selective blockage of the pore by Na^+, while the passage of K^+ is favored under high voltages as Na^+ no longer blocks the pore, but its stronger affinity for carboxylate groups slows its passage. In addition, under low voltages, the 3COO nanopore exhibits unusual conduction properties (*i.e.*, single-ion conduction with knock-on mechanism), which makes this nanopore act as a novel ion transporter or quanta arithmometer. This study demonstrates that the structures of biological channel proteins and the mechanisms for their functions indeed could provide inspirations and directions for the design of biomimetic devices to transplant their functions to practical applications, though sometimes it is difficult to reproduce the elaborate structures critical to their functions, such as the water bridge formed in NavAb selectivity filter cannot be replicated by the 4COO nanopore to achieve Na^+ selectivity. The design of biomimetic ion-selective nanopores, in turn, gives deeper insights into the ion selectivity mechanisms of biological ion channels. These biomimetic Na^+- or K^+-selective graphene nanopores have potential applications as sensitive ion sensors, novel nanofiltration devices for Na^+/K^+ separation, and as a voltage-switch machine to transport selected ions.

COMPUTATIONAL METHODS

Simulation Models and Details. The graphene nanopore was located at the center of a simulation box, dividing it into two compartments (Figure 1C). The simulation box was filled with 0.5 M NaCl and 0.5 M KCl mixture solution, comprising about 1670 water molecules, 15 Na^+, 15 K^+, and 30 Cl^-. For the 4COO and 3COO nanopores, one or two more Na^+ and K^+ ions were added to make the system electro-neutral.

In the simulations, the partial charges and parameters for the carbonyl groups and carboxylate groups were taken from the backbone carbonyl group and the side chain of glutamic acid in the CHARMM 27 force field,[77] respectively. Each carboxylate group $-COO^-$ carries a net charge of -1 *e*. All carbon atoms not in the functional groups were modeled as sp^2-like aromatic carbons in the CHARMM27 force field, and the TIP3P model[78] was used for water. The parameters for Na^+, K^+, and Cl^- were also taken from the CHARMM27 force field. After energy minimization, the system was equilibrated for 2 ns under NPT ensemble at 300 K and 1 atm to obtain proper water density in the system. The NVT ensemble was implemented in the subsequent simulations. The short-range van der Waals interactions were cut off at 1 nm. The long-range electrostatic interactions were computed with particle mesh Ewald method.[79] Periodic boundary conditions were imposed in all directions. Trajectories were integrated using the leapfrog scheme with a time step of 2 fs. Coordinates were stored every 1 ps. During the simulations, only the carbon atoms at the edges of the graphene sheet were fixed to keep the graphene at the center of the simulation box; the functional groups and other graphene carbon atoms were mobile.

Simulating Ion Conduction under Transmembrane Voltage Bias. During each ion conduction experiment, a uniform electric field E was applied along the positive direction of the z-axis to generate an effective transmembrane voltage bias V (Figure 1C) to drive ions through the nanopores.[72,73] The corresponding voltage bias was calculated *via* $V = -E \times L_z$, where L_z is the extent of the simulation box along the z-axis (4.36 nm). The first 5 ns is used as equilibration, and the data from the remainder (300 ns unless otherwise stated) were collected to analyze ion conduction. The simulation was divided into equal 100 ns blocks to calculate the error bars of ionic currents and K^+/Na^+ selectivity ratio of the nanopore. For these nanopores, E = 0, 0.01, 0.03, 0.05, 0.07, and 0.1 V/nm were used to generate voltages of V = 0, 0.0436, 0.1368, 0.218, 0.3052, and 0.436 V. Additional larger V = 0.654 and 0.872 V (corresponding E = 0.15 and 0.2 V/nm) were also applied in the 3COO nanopore system as it displayed lower currents. We note that the applied transmembrane voltage bias induces the formation of Cl^- concentration polarization layers on the right side of the graphene sheet (Figure S8 in the Supporting Information).

Potential of Mean Force (PMF) Calculation. The single-ion two-dimensional PMF in the axial and radial directions for Na^+ and K^+ passing through the nanopores was determined with umbrella sampling[80] in the absence of an electric field. In this method, a harmonic biasing potential was used to restrain the position of the ion along the reaction pathway defined by the axial distance (z) to the nanopore center and radial distance (r) to the nanopore axis. For the 4CO and 4COO nanopores, the target position of the ion was moved from $z = -1.5$ to $z = 1.5$ nm in 0.05 nm increments for both r = 0 and r = 0.5 nm using force constant 400 and 40 kJ/mol/nm^2 in the axial and radial directions, respectively. In addition, a larger constant of 400 kJ/mol/nm^2 in the radial direction was also used for r = 0 nm to better sample positions close to the nanopore axis; the radial position at r = 0.8 nm was also sampled for the 4COO nanopore due to its larger diameter. Each window was run for 1.5 ns, and the first 0.5 ns was excluded as equilibration. To test convergence, we ran a number of the PMF profiles for an additional 1.0 ns and found all points changed by less than 1.0 kJ/mol. Using the implementation by Grossfield,[81] the weighted histogram

analysis method[82] (WHAM) was used to calculate two-dimensional PMF with a tolerance of 10^{-5}; 150 and 40 bins were adopted in the axial and radial directions, respectively. The two-dimensional PMF was renormalized in the radial direction to account for the size of the volume element $2\pi r$. A one-dimensional PMF was obtained by integrating the normalized probabilities in $x-y$ plane up to $r = 0.8$ nm. All the simulations were performed with GROMACS4.5.5 software.[83] The PLUMED1.3.0 plug-in[84] was used for the two-dimensional PMF calculation. Coordination number calculations were based on the cutoffs of 0.32 and 0.36 nm for Na^+ and K^+, respectively.

Conflict of Interest: The authors declare no competing financial interest.

Acknowledgment. This work was supported by the National Key Basic Research Program of China (No. 2013CB733500), Program for New Century Excellent Talents in University (NCET-07-0313), National Natural Science Foundation of China (No. 21376089), Guangdong Science Foundation (No. S2011010002078), and the Fundamental Research Funds for the Central Universities (SCUT-2013ZM0073). The computational resources for this project are provided by SCUTGrid at South China University of Technology, the National Computational Infrastructure (NCI) National Facility (Australia), and iVEC. Z.H. thanks the China Scholarship Council for support.

Supporting Information Available: Additional figures and movies as noted in the text. This material is available free of charge *via* the Internet at http://pubs.acs.org.

REFERENCES AND NOTES

1. Hille, B. *Ionic Channels of Excitable Membranes*, 3rd ed.; Sinauer Associates Inc.: Sunderland, MA, 2001.
2. Agre, P. Aquaporin Water Channels (Nobel Lecture). *Angew. Chem., Int. Ed.* **2004**, *43*, 4278–4290.
3. MacKinnon, R. Potassium Channels and the Atomic Basis of Selective Ion Conduction (Nobel Lecture). *Angew. Chem., Int. Ed.* **2004**, *43*, 4265–4277.
4. Kumar, M.; Grzelakowski, M.; Zilles, J.; Clark, M.; Meier, W. Highly Permeable Polymeric Membranes Based on the Incorporation of the Functional Water Channel Protein Aquaporin Z. *Proc. Natl. Acad. Sci. U.S.A.* **2007**, *104*, 20719–20724.
5. Jovanovic-Talisman, T.; Tetenbaum-Novatt, J.; McKenney, A. S.; Zilman, A.; Peters, R.; Rout, M. P.; Chait, B. T. Artificial Nanopores That Mimic the Transport Selectivity of the Nuclear Pore Complex. *Nature* **2009**, *457*, 1023–1027.
6. Hou, X.; Yang, F.; Li, L.; Song, Y.; Jiang, L.; Zhu, D. A Biomimetic Asymmetric Responsive Single Nanochannel. *J. Am. Chem. Soc.* **2010**, *132*, 11736–11742.
7. Gong, X. J.; Li, J. C.; Xu, K.; Wang, J. F.; Yang, H. A Controllable Molecular Sieve for Na^+ and K^+ Ions. *J. Am. Chem. Soc.* **2010**, *132*, 1873–1877.
8. Hilder, T. A.; Gordon, D.; Chung, S.-H. Computational Modeling of Transport in Synthetic Nanotubes. *Nanomed. Nanotechnol. Biol. Med.* **2011**, *7*, 702–709.
9. Pongprayoon, P.; Beckstein, O.; Sansom, M. S. P. Biomimetic Design of a Brush-like Nanopore: Simulation Studies. *J. Phys. Chem. B* **2012**, *116*, 462–468.
10. Garcia-Fandino, R.; Sansom, M. S. P. Designing Biomimetic Pores Based on Carbon Nanotubes. *Proc. Natl. Acad. Sci. U.S.A.* **2012**, *109*, 6939–6944.
11. Zhou, X. B.; Liu, G. D.; Yamato, K.; Shen, Y.; Cheng, R. X.; Wei, X. X.; Bai, W. L.; Gao, Y.; Li, H.; Liu, Y.; *et al.* Self-Assembling Subnanometer Pores with Unusual Mass-Transport Properties. *Nat. Commun.* **2012**, *3*, 949.
12. Li, J. Y.; Gong, X. J.; Lu, H. J.; Li, D.; Fang, H. P.; Zhou, R. H. Electrostatic Gating of a Nanometer Water Channel. *Proc. Natl. Acad. Sci. U.S.A.* **2007**, *104*, 3687–3692.
13. Lee, C. Y.; Choi, W.; Han, J. H.; Strano, M. S. Coherence Resonance in a Single-Walled Carbon Nanotube Ion Channel. *Science* **2010**, *329*, 1320–1324.
14. Novoselov, K. S.; Geim, A. K.; Morozov, S. V.; Jiang, D.; Zhang, Y.; Dubonos, S. V.; Grigorieva, I. V.; Firsov, A. A. Electric Field Effect in Atomically Thin Carbon Films. *Science* **2004**, *306*, 666–669.
15. Banhart, F.; Kotakoski, J.; Krasheninnikov, A. V. Structural Defects in Graphene. *ACS Nano* **2011**, *5*, 26–41.
16. Fischbein, M. D.; Drndic, M. Electron Beam Nanosculpting of Suspended Graphene Sheets. *Appl. Phys. Lett.* **2008**, *93*, 113107.
17. Lemme, M. C.; Bell, D. C.; Williams, J. R.; Stern, L. A.; Baugher, B. W. H.; Jarillo-Herrero, P.; Marcus, C. M. Etching of Graphene Devices with a Helium Ion Beam. *ACS Nano* **2009**, *3*, 2674–2676.
18. Jiang, D. E.; Cooper, V. R.; Dai, S. Porous Graphene as the Ultimate Membrane for Gas Separation. *Nano Lett.* **2009**, *9*, 4019–4024.
19. Blankenburg, S.; Bieri, M.; Fasel, R.; Mullen, K.; Pignedoli, C. A.; Passerone, D. Porous Graphene as an Atmospheric Nanofilter. *Small* **2010**, *6*, 2266–2271.
20. Koenig, S. P.; Wang, L. D.; Pellegrino, J.; Bunch, J. S. Selective Molecular Sieving through Porous Graphene. *Nat. Nanotechnol.* **2012**, *7*, 728–732.
21. Cohen-Tanugi, D.; Grossman, J. C. Water Desalination across Nanoporous Graphene. *Nano Lett.* **2012**, *12*, 3602–3608.
22. Sun, P. Z.; Zhu, M.; Wang, K. L.; Zhong, M. L.; Wei, J. Q.; Wu, D. H.; Xu, Z. P.; Zhu, H. W. Selective Ion Penetration of Graphene Oxide Membranes. *ACS Nano* **2013**, *7*, 428–437.
23. Sint, K.; Wang, B.; Kral, P. Selective Ion Passage through Functionalized Graphene Nanopores. *J. Am. Chem. Soc.* **2008**, *130*, 16448–16449.
24. Garaj, S.; Liu, S.; Golovchenko, J. A.; Branton, D. Molecule-Hugging Graphene Nanopores. *Proc. Natl. Acad. Sci. U.S.A.* **2013**, *110*, 12192–12196.
25. Prasongkit, J.; Grigoriev, A.; Pathak, B.; Ahuja, R.; Scheicher, R. H. Theoretical Study of Electronic Transport through DNA Nucleotides in a Double-Functionalized Graphene Nanogap. *J. Phys. Chem. C* **2013**, *117*, 15421–15428.
26. Jeong, H.; Kim, H. S.; Lee, S. H.; Lee, D.; Kim, Y. H.; Huh, N. Quantum Interference in DNA Bases Probed by Graphene Nanoribbons. *Appl. Phys. Lett.* **2013**, *103*, 023701.
27. Sathe, C.; Zou, X. Q.; Leburton, J. P.; Schulten, K. Computational Investigation of DNA Detection Using Graphene Nanopores. *ACS Nano* **2011**, *5*, 8842–8851.
28. Wells, D. B.; Belkin, M.; Comer, J.; Aksimentiev, A. Assessing Graphene Nanopores for Sequencing DNA. *Nano Lett.* **2012**, *12*, 4117–4123.
29. LeMasurier, M.; Heginbotham, L.; Miller, C. Kcsa: It's a Potassium Channel. *J. Gen. Physiol.* **2001**, *118*, 303–313.
30. Favre, I.; Moczydlowski, E.; Schild, L. On the Structural Basis for Ionic Selectivity among Na^+, K^+, and Ca^{2+} in the Voltage-Gated Sodium Channel. *Biophys. J.* **1996**, *71*, 3110–3125.
31. Payandeh, J.; Scheuer, T.; Zheng, N.; Catterall, W. A. The Crystal Structure of a Voltage-Gated Sodium Channel. *Nature* **2011**, *475*, 353–358.
32. Doyle, D. A.; Cabral, J. M.; Pfuetzner, R. A.; Kuo, A. L.; Gulbis, J. M.; Cohen, S. L.; Chait, B. T.; MacKinnon, R. The Structure of the Potassium Channel: Molecular Basis of K^+ Conduction and Selectivity. *Science* **1998**, *280*, 69–77.
33. Zhou, Y. F.; Morais-Cabral, J. H.; Kaufman, A.; MacKinnon, R. Chemistry of Ion Coordination and Hydration Revealed by a K^+ Channel-Fab Complex at 2.0 Ångstrom Resolution. *Nature* **2001**, *414*, 43–48.
34. Jiang, Y. X.; Lee, A.; Chen, J. Y.; Cadene, M.; Chait, B. T.; MacKinnon, R. The Open Pore Conformation of Potassium Channels. *Nature* **2002**, *417*, 523–526.
35. McCusker, E. C.; Bagneris, C.; Naylor, C. E.; Cole, A. R.; D'Avanzo, N.; Nichols, C. G.; Wallace, B. A. Structure of a Bacterial Voltage-Gated Sodium Channel Pore Reveals Mechanisms of Opening and Closing. *Nat. Commun.* **2012**, *3*, 1102.
36. Zhang, X.; Ren, W. L.; DeCaen, P.; Yan, C. Y.; Tao, X.; Tang, L.; Wang, J. J.; Hasegawa, K.; Kumasaka, T.; He, J. H.; *et al.* Crystal Structure of an Orthologue of the Nachbac Voltage-Gated Sodium Channel. *Nature* **2012**, *486*, 130–134.
37. Bostick, D. L.; Brooks, C. L. Selectivity in K^+ Channels Is Due to Topological Control of the Permeant Ion's

Coordinated State. *Proc. Natl. Acad. Sci. U.S.A.* **2007**, *104*, 9260–9265.
38. Thomas, M.; Jayatilaka, D.; Corry, B. The Predominant Role of Coordination Number in Potassium Channel Selectivity. *Biophys. J.* **2007**, *93*, 2635–2643.
39. Varma, S.; Rempe, S. B. Tuning Ion Coordination Architectures To Enable Selective Partitioning. *Biophys. J.* **2007**, *93*, 1093–1099.
40. Varma, S.; Sabo, D.; Rempe, S. B. K^+/Na^+ Selectivity in K Channels and Valinomycin: Over-Coordination *versus* Cavity-Size Constraints. *J. Mol. Biol.* **2008**, *376*, 13–22.
41. Noskov, S. Y.; Berneche, S.; Roux, B. Control of Ion Selectivity in Potassium Channels by Electrostatic and Dynamic Properties of Carbonyl Ligands. *Nature* **2004**, *431*, 830–834.
42. Kim, I.; Allen, T. W. On the Selective Ion Binding Hypothesis for Potassium Channels. *Proc. Natl. Acad. Sci. U.S.A.* **2011**, *108*, 17963–17968.
43. Furini, S.; Domene, C. Atypical Mechanism of Conduction in Potassium Channels. *Proc. Natl. Acad. Sci. U.S.A.* **2009**, *106*, 16074–16077.
44. Jensen, M. O.; Borhani, D. W.; Lindorff-Larsen, K.; Maragakis, P.; Jogini, V.; Eastwood, M. P.; Dror, R. O.; Shaw, D. E. Principles of Conduction and Hydrophobic Gating in K^+ Channels. *Proc. Natl. Acad. Sci. U.S.A.* **2010**, *107*, 5833–5838.
45. Hille, B. The Permeability of the Sodium Channel to Metal Cations in Myelinated Nerve. *J. Gen. Physiol.* **1972**, *59*, 637–658.
46. Corry, B.; Thomas, M. Mechanism of Ion Permeation and Selectivity in a Voltage Gated Sodium Channel. *J. Am. Chem. Soc.* **2011**, *134*, 1840–1846.
47. Ke, S.; Zangerl, E. M.; Stary-Weinzinger, A. Distinct Interactions of Na^+ and Ca^{2+} Ions with the Selectivity Filter of the Bacterial Sodium Channel Na_VAb. *Biochem. Biophys. Res. Commun.* **2013**, *430*, 1272–1276.
48. Dudev, T.; Lim, C. Determinants of K^+ *vs* Na^+ Selectivity in Potassium Channels. *J. Am. Chem. Soc.* **2009**, *131*, 8092–8101.
49. Dudev, T.; Lim, C. Factors Governing the Na^+ *vs* K^+ Selectivity in Sodium Ion Channels. *J. Am. Chem. Soc.* **2010**, *132*, 2321–2332.
50. Thomas, M.; Jayatilaka, D.; Corry, B. Mapping the Importance of Four Factors in Creating Monovalent Ion Selectivity in Biological Molecules. *Biophys. J.* **2011**, *100*, 60–69.
51. Thomas, M.; Jayatilaka, D.; Corry, B. How Does Overcoordination Create Ion Selectivity? *Biophys. Chem.* **2013**, *172*, 37–42.
52. Thomas, M.; Jayatilaka, D.; Corry, B. An Entropic Mechanism of Generating Selective Ion Binding in Macromolecules. *PLoS Comput. Biol.* **2013**, *9*, e1002914.
53. Roux, B. Exploring the Ion Selectivity Properties of a Large Number of Simplified Binding Site Models. *Biophys. J.* **2010**, *98*, 2877–2885.
54. Noskov, S. Y.; Roux, B. Importance of Hydration and Dynamics on the Selectivity of the Kcsa and Nak Channels. *J. Gen. Physiol.* **2007**, *129*, 135–143.
55. Bagri, A.; Mattevi, C.; Acik, M.; Chabal, Y. J.; Chhowalla, M.; Shenoy, V. B. Structural Evolution during the Reduction of Chemically Derived Graphene Oxide. *Nat. Chem.* **2010**, *2*, 581–587.
56. Lu, N.; Wang, J. G.; Floresca, H. C.; Kim, M. J. *In Situ* Studies on the Shrinkage and Expansion of Graphene Nanopores under Electron Beam Irradiation at Temperatures in the Range of 400−1200 °C. *Carbon* **2012**, *50*, 2961–2965.
57. Shao, Q.; Zhou, J.; Lu, L. H.; Lu, X. H.; Zhu, Y. D.; Jiang, S. Y. Anomalous Hydration Shell Order of Na^+ and K^+ inside Carbon Nanotubes. *Nano Lett.* **2009**, *9*, 989–994.
58. Song, C.; Corry, B. Intrinsic Ion Selectivity of Narrow Hydrophobic Pores. *J. Phys. Chem. B* **2009**, *113*, 7642–7649.
59. He, Z. J.; Zhou, J. Steered Molecular Dynamics Simulations of Ions Traversing through Carbon Nanotubes. *Acta Chim. Sinica* **2011**, *69*, 2901–2907.
60. Zhu, Y. D.; Guo, X. J.; Shao, Q.; Wei, M. J.; Wu, X. M.; Lu, L. H.; Lu, X. H. Molecular Simulation Study of the Effect of Inner Wall Modified Groups on Ionic Hydration Confined in Carbon Nanotube. *Fluid Phase Equilib.* **2010**, *297*, 215–220.
61. He, Z. J.; Zhou, J.; Lu, X. H.; Corry, B. Ice-like Water Structure in Carbon Nanotube (8,8) Induces Cationic Hydration Enhancement. *J. Phys. Chem. C* **2013**, *117*, 11412–11420.
62. Ohba, T.; Hata, K.; Kanoh, H. Significant Hydration Shell Formation Instead of Hydrogen Bonds in Nanoconfined Aqueous Electrolyte Solutions. *J. Am. Chem. Soc.* **2012**, *134*, 17850–17853.
63. Zhu, Y.; Zhou, J.; Lu, X.; Guo, X.; Lu, L. Molecular Simulations on Nanoconfined Water Molecule Behaviors for Nanoporous Material Applications. *Microfluid. Nanofluid.* **2013**, *15*, 191–205.
64. Zhou, J.; Lu, X. H.; Wang, Y. R.; Shi, J. Molecular Dynamics Study on Ionic Hydration. *Fluid Phase Equilib.* **2002**, *194*, 257–270.
65. Egwolf, B.; Roux, B. Ion Selectivity of the Kcsa Channel: A Perspective from Multi-Ion Free Energy Landscapes. *J. Mol. Biol.* **2010**, *401*, 831–842.
66. Eisenman, G. Cation Selective Glass Electrodes and Their Mode of Operation. *Biophys. J.* **1962**, *2*, 259–323.
67. Noskov, S. Y.; Roux, B. Control of Ion Selectivity in Leut: Two Na^+ Binding Sites with Two Different Mechanisms. *J. Mol. Biol.* **2008**, *377*, 804–818.
68. Terekhova, I. V.; Romanova, A. O.; Kumeev, R. S.; Fedorov, M. V. Selective Na^+/K^+ Effects on the Formation of α-Cyclodextrin Complexes with Aromatic Carboxylic Acids: Competition for the Guest. *J. Phys. Chem. B* **2010**, *114*, 12607–12613.
69. Annapureddy, H. V. R.; Dang, L. X. Molecular Mechanism of Specific Ion Interactions between Alkali Cations and Acetate Anion in Aqueous Solution: A Molecular Dynamics Study. *J. Phys. Chem. B* **2012**, *116*, 7492–7498.
70. Jensen, M. O.; Jogini, V.; Borhani, D. W.; Leffler, A. E.; Dror, R. O.; Shaw, D. E. Mechanism of Voltage Gating in Potassium Channels. *Science* **2012**, *336*, 229–233.
71. Ulmschneider, M. B.; Bagneris, C.; McCusker, E. C.; DeCaen, P. G.; Delling, M.; Clapham, D. E.; Ulmschneider, J. P.; Wallace, B. A. Molecular Dynamics of Ion Transport through the Open Conformation of a Bacterial Voltage-Gated Sodium Channel. *Proc. Natl. Acad. Sci. U.S.A.* **2013**, *110*, 6364–6369.
72. Aksimentiev, A.; Schulten, K. Imaging α-Hemolysin with Molecular Dynamics: Ionic Conductance, Osmotic Permeability, and the Electrostatic Potential Map. *Biophys. J.* **2005**, *88*, 3745–3761.
73. Aksimentiev, A. Deciphering Ionic Current Signatures of DNA Transport through a Nanopore. *Nanoscale* **2010**, *2*, 468–483.
74. Furini, S.; Domene, C. On Conduction in a Bacterial Sodium Channel. *PLoS Comput. Biol.* **2012**, *8*, e1002476.
75. Stock, L.; Delemotte, L.; Carnevale, V.; Treptow, W.; Klein, M. L. Conduction in a Biological Sodium Selective Channel. *J. Phys. Chem. B* **2013**, *117*, 3782–3789.
76. Corry, B. Na^+/Ca^{2+} Selectivity in the Bacterial Voltage-Gated Sodium Channel Navab. *PeerJ* **2013**, 1, e16, DOI: 10.7717/peerj.16.
77. MacKerell, A. D.; Bashford, D.; Bellott, M.; Dunbrack, R. L.; Evanseck, J. D.; Field, M. J.; Fischer, S.; Gao, J.; Guo, H.; Ha, S.; *et al.* All-Atom Empirical Potential for Molecular Modeling and Dynamics Studies of Proteins. *J. Phys. Chem. B* **1998**, *102*, 3586–3616.
78. Jorgensen, W. L.; Chandrasekhar, J.; Madura, J. D.; Impey, R. W.; Klein, M. L. Comparison of Simple Potential Functions for Simulating Liquid Water. *J. Chem. Phys.* **1983**, *79*, 926–935.
79. Darden, T.; York, D.; Pedersen, L. Particle Mesh Ewald: An $N\cdot\log(N)$ Method for Ewald Sums in Large Systems. *J. Chem. Phys.* **1993**, *98*, 10089–10092.
80. Torrie, G. M.; Valleau, J. P. Monte-Carlo Free-Energy Estimates Using Non-Boltzmann Sampling: Application to Subcritical Lennard-Jones Fluid. *Chem. Phys. Lett.* **1974**, *28*, 578–581.
81. Grossfield, A. *WHAM: The Weighted Histogram Analysis Method*, version 2.0.6, http://membrane.urmc.rochester.edu/content/wham.

82. Kumar, S.; Bouzida, D.; Swendsen, R. H.; Kollman, P. A.; Rosenberg, J. M. The Weighted Histogram Analysis Method for Free-Energy Calculations on Biomolecules 0.1. The Method. *J. Comput. Chem.* **1992**, *13*, 1011–1021.
83. Hess, B.; Kutzner, C.; van der Spoel, D.; Lindahl, E. Gromacs 4: Algorithms for Highly Efficient, Load-Balanced, and Scalable Molecular Simulation. *J. Chem. Theory Comput.* **2008**, *4*, 435–447.
84. Bonomi, M.; Branduardi, D.; Bussi, G.; Camilloni, C.; Provasi, D.; Raiteri, P.; Donadio, D.; Marinelli, F.; Pietrucci, F.; Broglia, R. A.; *et al.* Plumed: A Portable Plugin for Free-Energy Calculations with Molecular Dynamics. *Comput. Phys. Commun.* **2009**, *180*, 1961–1972.